Superconductivity in the Nb-Ru-Ge σ phase

Elizabeth M. Carnicom,[1,*] Weiwei Xie,[2] Zuzanna Sobczak,[3] Tai Kong,[1] Tomasz Klimczuk,[3] and R. J. Cava[1,†]

[1]*Department of Chemistry, Princeton University, Princeton, New Jersey 08544, USA*

[2]*Department of Chemistry, Louisiana State University, Baton Rouge, Louisiana 70803, USA*

[3]*Department of Physics, Gdansk University of Technology, Gdansk 80-233, Poland*

(Received 29 September 2017; published 7 December 2017)

We show that the previously unreported ternary σ-phase material $Nb_{20.4}Ru_{5.7}Ge_{3.9}$ ($Nb_{0.68}Ru_{0.19}Ge_{0.13}$) is a superconductor with a critical temperature of 2.2 K. Temperature-dependent magnetic susceptibility, resistance, and specific-heat measurements were used to characterize the superconducting transition. The Sommerfeld constant γ for $Nb_{20.4}Ru_{5.7}Ge_{3.9}$ is 91 mJ mol f.u.$^{-1}$K^{-2} ($\sim$3 mJ mol atom^{-1} K^{-2}) and the specific-heat anomaly at the superconducting transition, $\Delta C/\gamma T_c$, is approximately 1.38. The zero-temperature upper critical field [$\mu_0 Hc_2(0)$] was estimated to be 2 T by resistance data. Field-dependent magnetization data analysis estimated $\mu_0 Hc_1(0)$ to be 5.5 mT. Thus, the characterization shows $Nb_{20.4}Ru_{5.7}Ge_{3.9}$ to be a type-II BCS superconductor. This material appears to be the first reported ternary phase in the Nb-Ru-Ge system, and the fact that there are no previously reported binary Nb-Ru, Nb-Ge, or Ru-Ge σ phases shows that all three elements are necessary to stabilize the material. An analogous σ phase in the Ta-Ru-Ge system did not display superconductivity above 1.7 K, which suggests that electron count cannot govern the superconductivity observed. Preliminary characterization of a possible superconducting σ phase in the Nb-Ru-Ga system is also reported.

DOI: 10.1103/PhysRevMaterials.1.074802

I. INTRODUCTION

The sigma (σ) phases, which are typically brittle, have been extensively studied in materials science due to their detrimental effects on the mechanical properties of various steels, although the precipitation of this phase in specific amounts can sometimes lead to hardening as well [1–5]. σ phases, which have tetragonal symmetry and adopt the CrFe structure type, have extremely broad compositional existence ranges and complex compositions as a common feature—extensive substitutions on one or more of the five crystallographically distinct sites in the crystal structure have been reported [1]. Due to this complexity, no unifying convention is yet available for depicting their compositions. We present the composition of the current material in terms of the number of atoms per unit cell (there are a total of 30), while also employing the atomic fractions for this and other systems for clarification [6].

σ phases are known to exist in over 40 different binary systems, and superconductivity has been observed in several of these [2,7]. $Nb_{0.65}Rh_{0.35}$, for example, has been reported to display superconductivity with a critical temperature (T_c) of 2.9 K [8] and $Nb_{0.62}Pt_{0.38}$ has a T_c of 2.1 K [9]. Differing T_c values have been observed based on the composition of the σ phase in both the Nb-Ir and Mo-Re binary systems [10,11]. The binary σ phase $Mo_{0.33}Re_{0.67}$ displays a T_c of 5.8 K, while $Mo_{0.50}Re_{0.50}$ has a T_c of 6.4 K [11,12]. For the Nb-Ir system, the literature values of T_c vary from 2 to 9 K for the σ phases [13–17]. The W-Os σ phase shows similar behavior, where T_c varies from 2.5 to 3.8 K as the osmium content is increased [12]. The changes in T_c based on composition for the σ phases are consistent with arguments that the critical temperature increases as the unit-cell volume decreases and the valence electron count per atom increases [12,15]. To the best of the authors' knowledge, superconductivity in ternary σ phases has not been previously reported.

Here we report the superconducting σ phase $Nb_{20.4}Ru_{5.7}Ge_{3.9}$ ($Nb_{0.68}Ru_{0.19}Ge_{0.13}$). This appears to be the first ternary phase in the Nb-Ru-Ge system, and no σ phase has been reported in the Nb-Ru, Nb-Ge, or Ru-Ge binary systems. Its superconducting transition is sharp and reproducible from one preparation to the next, and its powder x-ray-diffraction (pXRD) patterns show the appearance of second phases when deviations from this composition are made, and thus the material forms in a relatively narrow composition range. In addition, the fact that a σ phase has not been reported in the Ge-Ru, Nb-Ge, or Nb-Ru binary systems shows that all three elements are necessary for the existence of the σ-phase material in the ternary system. We present the crystal structure determined by single-crystal x-ray diffraction and characterize the superconducting transition through temperature-dependent magnetic susceptibility, resistance, and specific-heat measurements. All measurements consistently show a critical temperature of 2.2 K. Specific-heat data confirm that the transition is from the bulk of the material and $Nb_{20.4}Ru_{5.7}Ge_{3.9}$ appears to be a weak-coupled BCS-type superconductor. A Ta-Ru-Ge σ phase, with an approximate composition of $Ta_{20.4}Ru_{5.7}Ge_{3.9}$, was also synthesized, but did not display superconductivity above 1.7 K. We also present preliminary results of the possible 2-K superconductor in the Nb-Ru-Ga σ-phase system.

II. EXPERIMENT

The starting materials for the synthesis of polycrystalline $Nb_{20.4}Ru_{5.7}Ge_{3.9}$ (or the tantalum or gallium variants) were niobium (>99.9%, 325 mesh, Aldrich), tantalum (>99.9%, foil, 0.127 mm, Alfa), ruthenium (>99.9%, 200 mesh, Aldrich), germanium (>99.9%, 3.2 mm, Alfa), and gallium (>99.99%, pellet, 6-mm diameter, Aldrich). Niobium and ruthenium powders were pressed into pellets and first arc

*carnicom@princeton.edu

†rcava@exchange.princeton.edu

melted separately in order to avoid significant mass loss during melting with germanium. The niobium (or tantalum), ruthenium, and germanium chunks were then arc melted in a Zr-gettered atmosphere under ∼600 mbars Ar in a 6.8:1.9:1.3 (20.4:5.7:3.9) ratio. The purest sample for the Nb-Ru-Ga system resulted when the loading composition was $Nb_{20}Ru_5Ga_5$ ($Nb_{0.67}Ru_{0.165}Ga_{0.165}$). In addition, variation of the composition from the above formulas led to the presence of second phases in significant amounts. The arc-melted button was flipped over and remelted three times in order to ensure homogeneity throughout the sample. Mass loss after melting was <1%. Samples of $Nb_{20.4}Ru_{5.7}Ge_{3.9}$ are stable and do not decompose over time when exposed to air. Room-temperature pXRD was used to determine the purity of the samples using a Bruker D8 Advance Eco Cu K_α radiation ($\lambda = 1.5406$ Å) diffractometer equipped with a LynxEye-XE detector. Single crystals taken from the as-melted sample were mounted on the tips of Kapton loops and room-temperature intensity data were collected using a Bruker Apex II x-ray diffractometer with Mo Kα_1 radiation ($\lambda = 0.71073$ Å). All data were collected over a full sphere of reciprocal space with 0.5-deg scans in ω and an exposure time of 10 s per frame. The 2θ range was from 4 to 75 deg and the SMART software was used for acquiring all data. The SAINT program was used to extract intensities and correct for Lorentz and polarization effects. Numerical absorption corrections were done with XPREP, which is based on face-indexed absorption [18]. For the single-crystal refinement, the formula was constrained to the composition $Nb_{20.4}Ru_{5.7}Ge_{3.9}$ ($Nb_{0.68}Ru_{0.19}Ge_{0.13}$) since this loading composition resulted in a single phase sample and the arc-melting process had <1% mass loss. The crystal structure of $Nb_{20.4}Ru_{5.7}Ge_{3.9}$ was solved using direct methods and refined by full-matrix least squares on F^2 using the SHELXTL package [19]. All crystal structure drawings were created in the program VESTA [20]. A Rietveld refinement was performed on pXRD data with the FULLPROF Suite program using Thompson-Cox-Hastings pseudo-Voigt peak shapes. Parameters determined from the single-crystal refinement were used as a starting point for the powder refinement. Lattice parameters and site occupancies from both powder and single-crystal refinements are consistent with one another and therefore only the single-crystal data will be discussed here.

A Quantum Design physical property measurement system (PPMS) Dynacool equipped with vibrating sample magnetometer and resistivity options was used to measure the temperature- and field-dependent magnetization and temperature-dependent electrical resistance of $Nb_{20.4}Ru_{5.7}Ge_{3.9}$. A standard four-probe method was used for the temperature-dependent resistance measurement taken from 300 to 1.7 K with an applied current of 1 mA and applied magnetic fields ranging from 0 to 0.85 T. Zero-field-cooled (ZFC) and field-cooled (FC) magnetic susceptibility data were collected with an applied field of 10 Oe in the temperature range from 1.68 to 3.5 K. The field-dependent magnetization was measured at various temperatures from 1.68 to 2.2 K with a field sweep from 0 to 100 Oe. A Quantum Design PPMS Evercool II was also used to measure the heat capacity on a small crystal of $Nb_{20.4}Ru_{5.7}Ge_{3.9}$ with 0-, 0.1-, 0.2-, 0.3-, and 0.4-T applied fields.

TABLE I. Single-crystal crystallographic data for $Nb_{20.4}Ru_{5.7}Ge_{3.9}$ at 300(2) K.

Chemical formula	$Nb_{20.4}Ru_{5.7}Ge_{3.9}$
F.W. (g/mol)	2754.63
Space group; Z	$P4_2/mnm$(No.136); 1
a (Å)	9.843(1)
c (Å)	5.1270(8)
V (Å^3)	496.7(2)
hkl	$-14 \leqslant hk \leqslant 14$ $-6 \leqslant l \leqslant 6$
Absorption correction	Numerical
Extinction coefficient	0.0006(2)
θ range (deg)	2.927–32.044
No. reflections; R_{int}	1613; 0.1114
No. independent reflections	472
No. parameters	27
R_1; wR_2 ($I > 2\delta(I)$)	0.0650; 0.1073
R_1; wR_2 (all I)	0.1246; 0.1287
Goodness of fit	1.038
Diffraction peak and hole (e^-/Å^3)	4.249; −2.985

III. RESULTS AND DISCUSSION

Powder x-ray diffraction and single-crystal x-ray diffraction were used to analyze the crystal structure of the previously unreported σ phase $Nb_{20.4}Ru_{5.7}Ge_{3.9}$ ($Nb_{0.68}Ru_{0.19}Ge_{0.13}$). It crystallizes in the CrFe structure type ($P4_2/mnm$, No. 136) with lattice parameters $a = 9.843(1)$ Å and $c = 5.1270(8)$ Å. Table I shows a summary of the results from single-crystal diffraction data, and Table II gives the atomic coordinates determined from the structure refinement. Figure 1 shows the room-temperature powder-diffraction pattern of $Nb_{20.4}Ru_{5.7}Ge_{3.9}$ with the corresponding Rietveld fit to the data

TABLE II. Atomic coordinates and equivalent isotropic displacement parameters of $Nb_{20.4}Ru_{5.7}Ge_{3.9}$ at 300(2) K. U_{eq} is defined as one-third of the trace of the orthogonalized U_{ij} tensor (Å^2).

Atom	Wyckoff position	Occupancy	x	y	z	U_{eq}
Ru/Ge1/Nb4	2a	0.67(1)/0.23/0.1	0	0	0	0.006(1)
Ru/Ge2/Nb5	8j	0.54(5)/0.43/0.025	0.1825(2)	0.1825(2)	0.2506(6)	0.0049(6)
Nb1	4f	1	0.3961(2)	0.3961(2)	0	0.0072(8)
Nb2	8i_2	1	0.7414(2)	0.0670(3)	0	0.0047(5)
Nb3	8i_1	1	0.4647(2)	0.1280(2)	0	0.0043(6)

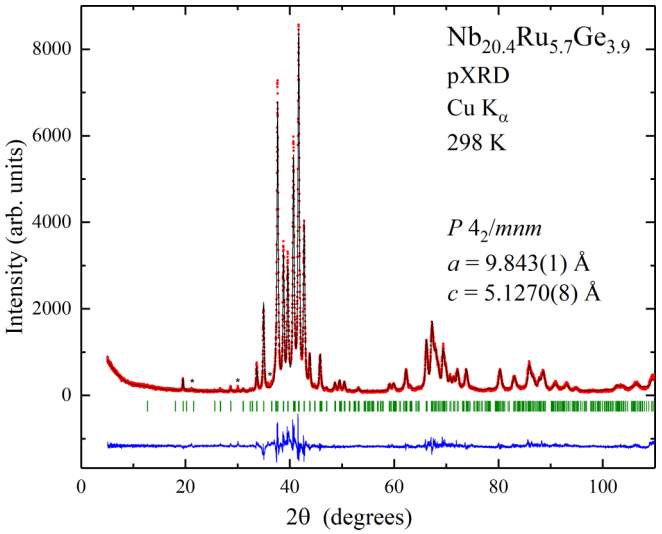

FIG. 1. Rietveld refinement of $Nb_{20.4}Ru_{5.7}Ge_{3.9}$ using room-temperature pXRD data. The experimentally observed data are shown in red circles, the calculated pattern is shown with a black line, the green vertical marks indicate expected Bragg reflections, and the blue line at the bottom shows the difference between the observed and calculated data. Impurity peaks are marked with asterisks. Rietveld refinement results: $\chi^2 = 3.53$; $wR_p = 13.6\%$; $R_p = 11.6\%$; $R(F^2) = 8.36\%$. The cluster of strong peaks near $2\theta = 40$ deg is a characteristic of σ phases.

confirming the high purity of the as-melted sample. The crystal structure of this new σ phase viewed along the c direction is presented in Fig. 2 showing the topologically closest packed structure, a common feature of σ phases [21–23].

Binary σ phases have the general formula A_2B (normalized here to $A_{20}B_{10}$ to reflect the unit-cell content). A is typically an early transition element with a preference for sites with higher coordination number (CN) such as the $4f$, $8i_1$, and $8j$ in the σ-phase structure. In contrast, the B atoms are typically more d-electron rich with a preference for lower CN sites like the $2a$ and $8i_2$ sites in the σ-phase structure. Ternary systems become more complicated, especially when a main group element like Ga, Al, or Si is included. When there are three elements present, it is necessary to do experiments with multiple wavelengths of radiation to quantitatively determine multiple site occupancies by diffraction. However, for our purposes, since the loading composition, $Nb_{20.4}Ru_{5.7}Ge_{3.9}$, resulted in a single-phase diffraction pattern and the mass loss was <1% following arc melting, the single-crystal refinement was constrained to the chemical formula of the loading composition. The phase presented here, $Nb_{20.4}Ru_{5.7}Ge_{3.9}$, has the sites $4f$, $8i_1$, and $8i_2$ (20 atoms total) fully occupied by Nb, with a small amount (0.4) of Nb evenly distributed across the $2a$ and $8j$ sites, while Ru and Ge, the "B atoms" are mixed in different ratios on the $2a$ and $8j$ sites (ten atoms total). Site mixing is commonly seen in σ phases, as previously stated. For example, $Nb_{18}Ni_3Al_9$ ($Nb_{0.6}Ni_{0.1}Al_{0.3}$) [24], $Cr_{13.5}Fe_{13.5}Si_3$ ($Cr_{0.45}Fe_{0.45}Si_{0.1}$) [25], $Mo_{12}Ru_{12}Ta_6$ ($Mo_{0.4}Ru_{0.4}Ta_{0.2}$) [26], and $Nb_{18}Mn_6Ga_6$ ($Nb_{0.6}Mn_{0.2}Ga_{0.2}$) [27] all form the σ phase but clearly have quite different combinations of elements and degrees of mixing. In addition, the examples above show that simple A and B element assignments are not always followed in these ternary σ phases. Although there are numerous previously reported ternary σ phases containing all transition metals [28,29] or two transition metals with Ga [27,30,31], Al [24,32,33], or Si [25,34] as the third element, to the best of our knowledge there are no previously reported ternary σ phases containing Ge, despite the close proximity to Al, Si, and Ga in the periodic table. In addition, the higher percentage of Nb, due to the full occupancy on the $4f$, $8i_1$, and $8i_2$ sites, is similar to the binary σ-phase superconductors $Nb_{0.65}Rh_{0.35}$ [8] and $Nb_{0.62}Pt_{0.38}$ [9], and could help to explain why superconductivity is seen in this new ternary σ phase.

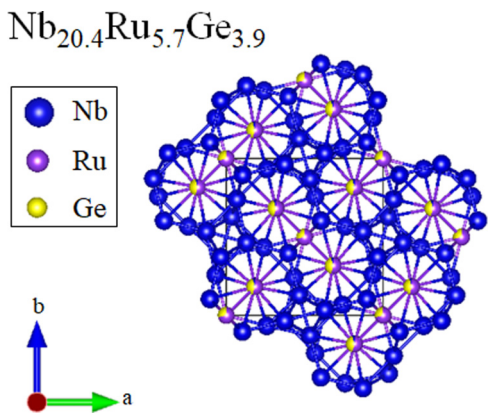

FIG. 2. Crystal structure of $Nb_{20.4}Ru_{5.7}Ge_{3.9}$ viewed along the c direction emphasizing the topologically closest packed structure. Niobium is shown in blue, ruthenium is shown in purple, and germanium is shown in yellow.

The temperature-dependent magnetic susceptibility (χ_v) is shown in Fig. 3 for $Nb_{20.4}Ru_{5.7}Ge_{3.9}$, measured in an

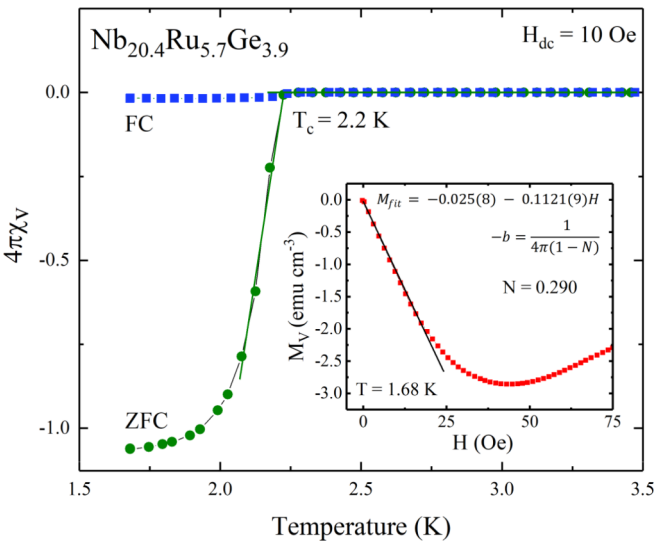

FIG. 3. Zero-field-cooled and field-cooled temperature-dependent magnetic susceptibility χ_V (T) measured in a 10-Oe applied magnetic field from 1.68 to 3.5 K showing the superconducting transition at 2.2 K. The data were corrected for the demagnetization factor, N. Inset: Field-dependent magnetization measured at the lowest possible temperature, 1.68 K, to estimate the value of the demagnetization factor.

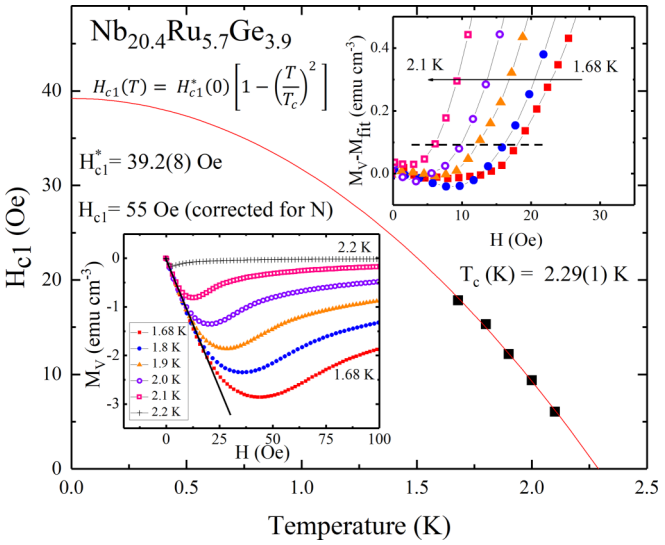

FIG. 4. The estimation of H_{c1}^{*} from the M_V-$M_{\rm fit}$ plot. Lower left inset: Magnetization (M_V) vs applied field (H) for the superconductor $Nb_{20.4}Ru_{5.7}Ge_{3.9}$ at temperatures between 1.68 and 2.2 K with a field sweep from 0 to 100 Oe. Upper right inset: The difference between the magnetization (M_V) and the $M_{\rm fit}$ at different temperatures.

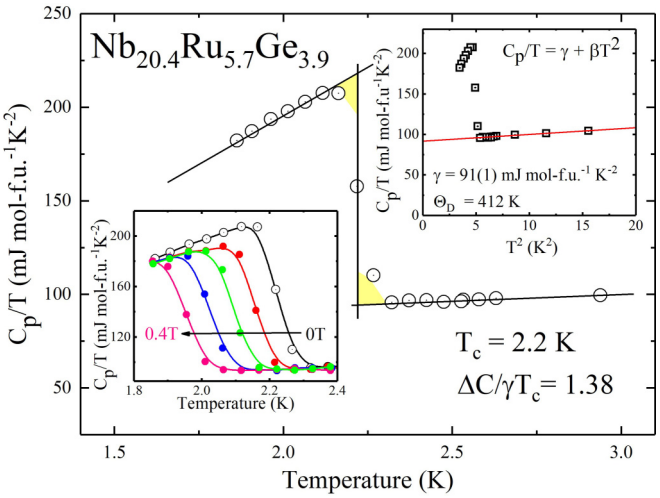

FIG. 5. C_p/T vs T plotted from 1.8 to 3 K measured in zero applied field where the solid black lines outline the equal area construction shown in yellow shading. Lower left inset: C_p/T vs T for various applied magnetic fields ranging from 0 to 0.4 T increasing by 0.1-T increments. Upper right inset: C_p/T vs T^2 plotted in the low-temperature region fitted to a line.

applied magnetic field of $H = 10$ Oe. The ZFC volume magnetic susceptibility data are only slightly less than the ideal $4\pi\chi_v = -1$ at the lowest possible temperature 1.68 K. Both the ZFC and FC magnetic susceptibility data were corrected for a demagnetization factor (a correction for the sample shape) N equal to 0.290. The value N was calculated from the fit ($M_{\rm fit}$) to the magnetization vs applied field measurements taken at 1.68 K at low fields, from 0 to 15 Oe, as shown in Fig. 3 (inset). Assuming linear behavior of M_V vs H in the superconducting state, the demagnetization factor can be calculated by the equation $-b = \frac{1}{4\pi(1-N)}$, where b is the slope of the linear fit and hence χ_V.

Figure 4 shows the characterization of the $Nb_{20.4}Ru_{5.7}Ge_{3.9}$ superconductor with field-dependent magnetization measurements. The lower left inset of Fig. 4 shows data taken at different temperatures ranging from 1.68 to 2.2 K with field sweeps from 0 to 100 Oe. The difference between the magnetization (M_V) and the $M_{\rm fit}$ measured at 1.68 K is shown in Fig. 4 (upper right inset). The fields (H) at which there is a deviation from linearity, indicated by the dashed line, were used to construct the plot in Fig. 4 (main panel) plotted as a function of temperature. The H_{c1} vs T data were fitted to the following equation:

$$H_{c1}(T) = H_{c1}^{*}(0)\left[1 - \left(\frac{T}{T_c}\right)^2\right]$$

where $H_{c1}^{*}(0)$ is the uncorrected lower critical field at 0 K and T_c is the calculated critical temperature. The lower critical field, $H_{c1}^{*}(0)$, was calculated to be 39.2(8) Oe and, after correcting for the demagnetization factor ($N = 0.290$), $H_{c1}(0) = 55$ Oe. The calculated T_c value was 2.29(1) K, consistent with the T_c from both temperature-dependent specific-heat data and resistance data, which will be discussed next.

Temperature-dependent specific-heat measurements were carried out as presented in Fig. 5 (main panel), which plots C_p/T vs T in zero applied field near the transition temperature. The large anomaly in the specific heat is consistent with bulk superconductivity in $Nb_{20.4}Ru_{5.7}Ge_{3.9}$. The superconducting T_c value was determined by equal-entropy constructions of the idealized specific-heat capacity jump (shown with yellow shading), which is sharp in temperature. The T_c of $Nb_{20.4}Ru_{5.7}Ge_{3.9}$ was determined to be 2.2 K, consistent with both the resistance and magnetic susceptibility data. The lower left inset of Fig. 5 shows the temperature dependence of the specific-heat data in applied magnetic fields from 0 to 0.4 T with 0.1-T increments. The T_c is suppressed to lower temperature as the applied field is increased, as expected.

The upper right inset of Fig. 5 shows a plot of C_p/T vs T^2 which was fitted to the equation

$$\frac{C_p}{T} = \gamma + \beta T^2,$$

where βT^3 is the phonon contribution and γT is the electronic contribution to the specific heat. The Sommerfeld parameter γ was calculated to be 91(1) mJ mol f.u.$^{-1}$ K^{-2} (~3 mJ mol atom^{-1} K^{-2}) and β was 0.831(5) mJ mol f.u.$^{-1}$ K^{-4} based on the slope of the fitted line. The Debye temperature Θ_D can then be calculated using β with the following equation:

$$\Theta_D = \left(\frac{12\pi^4}{5\beta} nR\right)^{1/3},$$

where R is the gas constant 8.314 J mol^{-1} K^{-1} and $n = 30$ for $Nb_{20.4}Ru_{5.7}Ge_{3.9}$. Based on this Debye model, Θ_D was calculated to be 412 K. It is worth noting that the Debye temperatures for elemental Ru and Ge are 600 and 374 K, respectively [35]. The Θ_D and determined T_c value can then

be used to calculate the electron-phonon coupling constant λ_{ep} from the inverted McMillan [36] formula as follows:

$$\lambda_{ep} = \frac{1.04 + \mu^* \ln\left(\frac{\Theta_D}{1.45T_c}\right)}{(1 - 0.62\mu^*)\ln\left(\frac{\Theta_D}{1.45T_c}\right) - 1.04}.$$

Assuming $\mu^* = 0.13$ and $T_c = 2.2$ K, λ_{ep} was calculated to be 0.49, which suggests that $Nb_{20.4}Ru_{5.7}Ge_{3.9}$ is a weak-coupling superconductor. The Fermi energy $N(E_F)$ can be calculated using the equation

$$N(E_F) = \frac{3\gamma}{\pi^2 k_B^2 (1 + \lambda_{ep})},$$

where k_B is the Boltzmann constant and $\gamma = 91(1)$ mJ mol f.u.$^{-1}$ K^{-1}. The estimated $N(E_F) = 39$ states eV^{-1} per formula unit of $Nb_{20.4}Ru_{5.7}Ge_{3.9}$. The specific-heat jump at transition to the superconducting state $\Delta C/T_c$ was calculated to be 123 mJ mol f.u^{-1} K^{-2} and $\Delta C/\gamma T_c = 1.38$, which is close to the expected value of 1.43, confirming bulk superconductivity in $Nb_{20.4}Ru_{5.7}Ge_{3.9}$.

The temperature-dependent normalized electrical resistance R/R_{300K} for a polycrystalline, irregularly shaped sample of $Nb_{20.4}Ru_{5.7}Ge_{3.9}$ measured from 300 to 1.7 K is shown in Fig. 6 (lower left inset). The resistance is relatively temperature independent in the entire temperature range from 2.3 to 300 K, most likely due to the large extent of mixing disorder in this new material; the σ phase in this system is a poor metal. In zero applied magnetic field, the resistance drops to zero, resulting in a T_c of 2.2 K for the superconductor. There is also a slight increase in the resistance slightly above T_c where the resistance

TABLE III. Superconductivity parameters of $Nb_{20.4}Ru_{5.7}Ge_{3.9}$.

Parameter	Units	$Nb_{20.4}Ru_{5.7}Ge_{3.9}$
T_c	K	2.2
$\mu_0 H_{c1}(0)$	mT	5.5
$\mu_0 H_{c2}(0)$	T	2.11
$\mu_0 H_c(0)$	mT	60
ξ_{GL}	Å	125
λ_{GL}	Å	3115
κ_{GL}		25
γ	mJ mol f.u.$^{-1}$ K^{-2}	91
$\Delta C/\gamma T_c$		1.38
$\mu_0 H^{Pauli}$	T	4.1
λ_{ep}		0.49
$N(E_F)$	states eV^{-1} per f.u.	39
Θ_D	K	412

is ~1.0 throughout the entire temperature range but jumps up to 1.1 at about 2.3 K. This behavior has been previously observed in other superconductors [37–39], and is most likely inherent of the material and not caused by the experimental setup. Figure 6 (upper right inset) shows the dependence of the critical temperature on the applied magnetic field, where T_c was taken as 50% of the superconducting transition (dashed line). The critical temperature decreases steadily as the applied field increases from 0 to 0.85 T where the T_c is suppressed to approximately 1.71 K when $\mu_0 H = 0.80$ T. The superconducting transition remains narrow in temperature for all fields studied. The estimated T_c values from the midpoints of resistance measurements were plotted (Fig. 6, main panel)

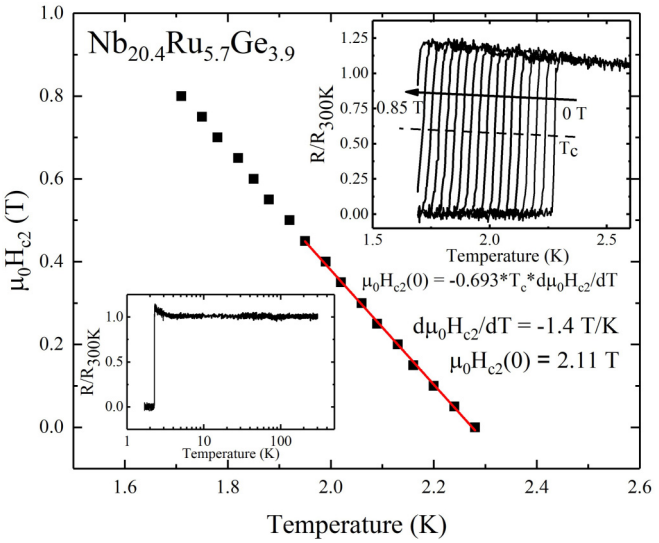

FIG. 6. Plot of H_{c2}(T) obtained from resistance data which were fitted to a line, resulting in a calculated value of $\mu_0 H_{c2}(0) = 2.11$ T. Lower left inset: Temperature-dependent electrical resistance normalized as R/R_{300K} measured over the temperature range 1.7–300 K with no applied field plotted on a log scale. Upper right inset: Dependence of superconducting transition on applied magnetic field plotted as the normalized resistance (R/R_{300K}) from 1.7 to 2.75 K in applied magnetic fields ranging from $\mu_0 H = 0$ to 0.85 T in steps of 0.05 T. The dashed line represents 50% of the superconducting transition.

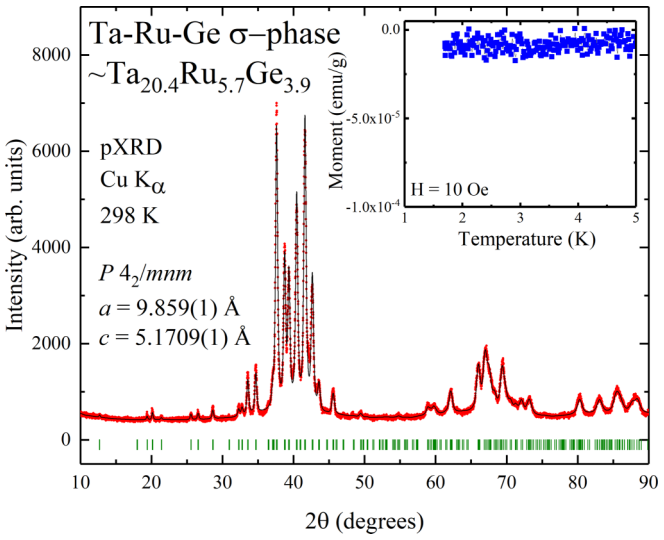

FIG. 7. Room-temperature pXRD pattern showing a LeBail fit of the σ phase in the Ta-Ru-Ge system, ~ $Ta_{20.4}Ru_{5.7}Ge_{3.9}$. Experimentally observed data are shown in red circles, the calculated diffraction pattern is shown with a black line, and the green vertical marks indicate expected Bragg reflections. Inset: Zero-field-cooled temperature-dependent magnetic susceptibility data measured from 1.7 to 5 K with a $H = 10$-Oe applied magnetic field, showing that the Ta-Ru-Ge σ phase is not superconducting down to 1.7 K.

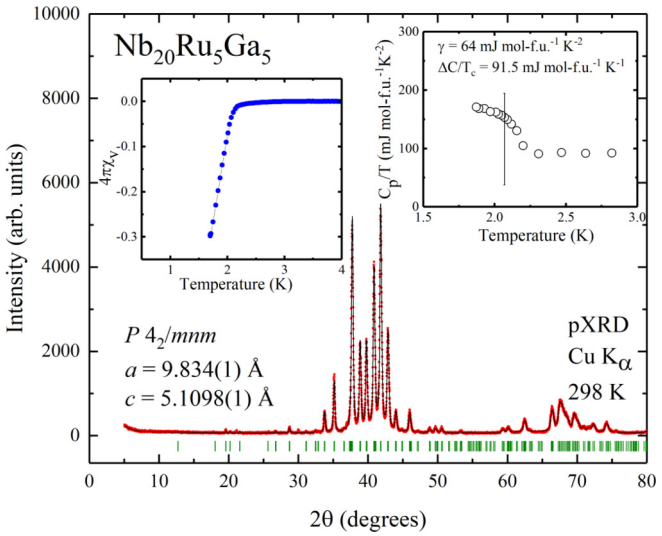

FIG. 8. Room-temperature pXRD pattern showing a LeBail fit of the σ phase $Nb_{20}Ru_5Ga_5$. Experimentally observed data are shown in red circles, the calculated diffraction pattern is shown with a black line, and the green vertical marks indicate expected Bragg reflections for space group $P4_2/mnm$. Right inset: Preliminary temperature-dependent specific heat data showing an anomaly in the specific heat at ~2 K. Left inset: Zero-field-cooled temperature-dependent magnetic susceptibility data showing an incomplete superconducting transition at ~2 K.

and fit to a line ($d\mu_0 H_{c2}/dT = -1.4\,\mathrm{T/K}$). By using the equation

$$\mu_0 H_{c2}(0) = -AT_c \left.\frac{d\mu_0 H_{c2}}{dT}\right|_{T=T_c},$$

where $T_c = 2.2\,\mathrm{K}$ and A is 0.69 for the dirty limit or 0.73 for the clean limit [40], $\mu_0 H_{c2}(0)$ was calculated to be 2.11 and 2.25 T for the dirty and clean limit of $Nb_{20.4}Ru_{5.7}Ge_{3.9}$, respectively. Both values are lower than the Pauli limit $\mu_0 H^{\mathrm{Pauli}} = 1.85^* T_c = 4.1\,\mathrm{T}$. The Ginzburg-Landau superconducting coherence length ξ_{GL} was estimated to be 125 Å from the equation

$$H_{c2}(0) = \frac{\Phi_0}{2\pi\xi_{\mathrm{GL}}^2},$$

where $\Phi_0 = h/2e$ and $\mu_0 H_{c2}(0) = 2.11\,\mathrm{T}$. The lower critical field, $H_{c1}(0) = 55\,\mathrm{Oe}$, was used with $\xi_{\mathrm{GL}} = 125$ Å to estimate the superconducting penetration depth λ_{GL} to be 3115 Å using the formula

$$H_{c1} = \frac{\Phi_0}{4\pi\lambda_{\mathrm{GL}}^2} \ln\frac{\lambda_{\mathrm{GL}}}{\xi_{\mathrm{GL}}}.$$

The ratio of the calculated values of λ_{GL} and ξ_{GL} will give the value $\kappa_{\mathrm{GL}} = 25$ [$\kappa_{\mathrm{GL}} = \lambda_{\mathrm{GL}}/\xi_{\mathrm{GL}}$], confirming type-II superconductivity in $Nb_{20.4}Ru_{5.7}Ge_{3.9}$. In addition, the κ_{GL} value can be used in the equation

$$H_{c1} H_{c2} = H_c^2 \ln\kappa_{\mathrm{GL}}$$

to calculate the thermodynamic critical field $\mu_0 H_c = 60\,\mathrm{mT}$. A summary of all superconducting parameters is given in Table III. A Ta-Ru-Ge σ phase, with an approximate composition of $Ta_{20.4}Ru_{5.7}Ge_{3.9}$, was synthesized as shown in Fig. 7 (main panel). The Ta-variant σ phase was tested for superconductivity but did not display superconductivity above 1.7 K (Fig. 7, inset). This suggests that electron count does not strictly govern the superconducting transition temperature seen in σ phases. Measurement of the specific heat for the Ta variant may be of interest to determine whether its density of states is substantially lower than that of the Nb variant. Finally, in Fig. 8, we show preliminary powder x-ray diffraction (main panel), magnetic susceptibility (left inset), and specific-heat data (right inset) for the σ phase in the Nb-Ru-Ga system, the composition of which is $Nb_{20}Ru_5Ga_5$ ($Nb_{0.67}Ru_{0.165}Ga_{0.165}$), suggesting that the presence of Nb is crucial for the superconductivity to be observed above 2 K. The superconducting T_c appears to be 2.1 K. Lower-temperature measurements would be required to fully characterize the superconducting transition in this material.

IV. CONCLUSIONS

We report the ternary σ-phase superconductor $Nb_{20.4}Ru_{5.7}Ge_{3.9}$, which has the σ-phase CrFe structure type ($P4_2/mnm$, No. 136). To the best of our knowledge, $Nb_{20.4}Ru_{5.7}Ge_{3.9}$ is the first ternary σ phase that is superconducting. Single-crystal diffraction studies showed that Nb fully occupies the $4f$, $8i_1$, and $8i_2$ sites, a small amount of Nb was evenly distributed on the $8j$ and $2a$ sites, while there is Ru/Ge mixing on the remaining $2a$ and $8j$ sites. Temperature-dependent magnetic susceptibility, resistance, and specific-heat measurements show that the material enters the superconducting state below a critical temperature of 2.2 K and that the superconductivity is an intrinsic property of the material. Based on the calculated superconducting parameters, $Nb_{20.4}Ru_{5.7}Ge_{3.9}$ is a weak-coupling type-II BCS superconductor. The σ phase with approximate composition $Ta_{20.4}Ru_{5.7}Ge_{3.9}$ was synthesized but does not display superconductivity above 1.7 K. We also present preliminary specific-heat, pXRD, and magnetic susceptibility results for the potential 2-K superconductor $Nb_{20}Ru_5Ga_5$. Measurements down to 0.4 K would be of interest for future work to fully characterize this possible superconductor. Thus, though the T_c values are low, our results combined with those in the literature for binary alloys suggest that σ-phase alloys appear to be favorable hosts for superconductivity.

ACKNOWLEDGMENTS

The materials synthesis was supported by the Department of Energy, Division of Basic Energy Sciences, Grant No. DE-FG02-98ER45706, and the property characterization was supported by the Gordon and Betty Moore Foundation EPiQS initiative, Grant No. GBMF-4412. The work at Louisiana State University (LSU) was supported by start-up funding through the LSU College of Science. The research in Poland was supported by the National Science Centre, Grant No. UMO-2016/22/M/ST5/00435.

[1] E. O. Hall and S. H. Algie, Metall. Rev. **11**, 61 (1966).
[2] J. M. Joubert, Prog. Mater. Sci. **53**, 528 (2008).
[3] L. K. Singhal and J. W. Martin, Acta Metall. **16**, 1441 (1968).
[4] C.-C. Hsieh and W. Wu, ISRN Metall. **2012**, 1 (2012).
[5] S. S. M. Tavares, J. M. Pardal, J. L. Guerreiro, A. M. Gomes, and M. R. da Silva, J. Magn. Magn. Mater. **322**, L29 (2010).
[6] E. M. Carnicom, W. Xie, T. Klimczuk, and R. J. Cava, Dalton Trans. **46**, 14158 (2017).
[7] B. W. Roberts, *Intermetallic Compounds* (Wiley, New York, 1967).
[8] H. R. Khan, K. Lüders, C. J. Raub, and G. Roth, Z. Phys. B **38**, 27 (1980).
[9] H. R. Khan, C. J. Raub, K. Lüders, and Z. Szücs, Appl. Phys. **15**, 307 (1978).
[10] H. R. Khan, C. J. Raub, K. Lüders, and G. Roth, J. Less-Common Met. **69**, 361 (1980).
[11] C. C. Koch and J. O. Scarbrough, Phys. Rev. B **3**, 742 (1971).
[12] R. D. Blaugher, A. Taylor, and J. K. Hulm, IBM J. Res. Dev. **6**, 116 (1962).
[13] V. B. Compton, E. Corenzqit, J. P. Maita, B. T. Matthias, and F. J. Morin, Phys. Rev. **123**, 1567 (1961).
[14] E. Bucher, F. Heininger, and J. Müller, in *Proceedings of the 8th International Conference on Low Temperature Physics* (Butterworths, Washington, DC, 1962), p. 153.
[15] R. D. Blaugher and J. K. Hulm, J. Chem. Solids **19**, 134 (1961).
[16] H. R. Khan, C. J. Raub, K. Lüders, and Z. Szücs, Appl. Phys. **19**, 231 (1979).
[17] H. R. Khan, C. J. Raub, K. Lüders, and Z. Szücs, Appl. Phys. **13**, 123 (1977).
[18] SHELXTL, Software Reference Manual, Version 6.10, Bruker Analytical X-Ray Systems, Inc., Madison, WI, 2000.
[19] G. M. Sheldrick, Acta Crystallogr. Sect. A **64**, 112 (2008).
[20] K. Momma and F. Izumi, J. Appl. Crystallogr. **44**, 1272 (2011).
[21] J. S. Kasper and R. M. Waterstrat, Acta Crystallogr. **9**, 289 (1956).
[22] F. C. Frank and J. S. Kasper, Acta Crystallogr. **12**, 483 (1959).
[23] F. C. Frank and J. S. Kasper, Acta Crystallogr. **11**, 184 (1958).
[24] C. R. J. Hunt and A. Raman, Z. Metallkde. **59**, 701 (1968).
[25] Y. I. Gladyshevskiy and L. K. Borusevich, Russ. Metall. **1966**, 87 (1966).
[26] I. M. Subbotin, M. V. Raevskaya, T. P. Loboda, and E. M. Sokolovskaya, Moscow Univ. Chem. Bull. **36**, 51 (1981).
[27] M. T. Orillion and A. Raman, Z. Metallkde. **65**, 709 (1974).
[28] K. Yaqoob, J. C. Crivello, and J. M. Joubert, Inorg. Chem. **51**, 3071 (2012).
[29] H. Martens and P. Duwez, Trans. Am. Soc. Met. **44**, 484 (1952).
[30] A. Bezinge, K. Yvon, and J. Müller, J. Less-Common Met. **98**, L9 (1984).
[31] M. Dryś, J. Less-Common Met. **75**, 261 (1980).
[32] R. C. Hansen and A. Raman, Z. Metallkde. **61**, 115 (1970).
[33] S. Samuha, D. Pavlyuchkov, O. V. Zaikina, B. Grushko, and L. Meshi, J. Alloys Compd. **621**, 47 (2015).
[34] K. P. Gupta, N. S. Rajan, and P. A. Beck, Trans. Metall. Soc. AIME **218**, 617 (1960).
[35] C. Kittel, *Introduction to Solid State Physics*, 8th ed. (Wiley, New York, 2005).
[36] W. L. McMillan, Phys. Rev. **167**, 331 (1968).
[37] T. Klimczuk, T. Plackowski, W. Sadowski, and M. Plebańczyk, Phys. C Supercond. **387**, 203 (2003).
[38] M. A. Crusellas, J. Fontcuberta, and S. Piñol, Phys. Rev. B **46**, 14089 (1992).
[39] C. R. Rotundu, V. V. Struzhkin, M. S. Somayazulu, S. Sinogeikin, R. J. Hemley, and R. L. Greene, Phys. Rev. B **87**, 024506 (2013).
[40] N. R. Werthamer, E. Helfand, and P. C. Hohenberg, Phys. Rev. **147**, 295 (1966).